Dissipative Control for Physical Human–Robot Interaction

Stuart A. Bowyer, *Member, IEEE*, and Ferdinando Rodriguez y Baena, *Member, IEEE*

Abstract—Physical human–robot interaction is fundamental to exploiting the capabilities of robots in tasks and environments where robots have limited cognition or comprehension and is virtually ubiquitous for robotic manipulation in highly unstructured environments, as are found in surgery. A critical aspect of physical human–robot interaction in these cases is controlling the robot so that the individual human and robot competencies are maximized, while guaranteeing user, task, and environment safety. Dissipative control precludes dangerous forcing of a shared tool by the robot, ensuring safety; however, it typically suffers from poor control fidelity, resulting in reduced task accuracy. In this study, a novel, rigorously formalized, n-dimensional dissipative control strategy is proposed that employs a new technique called "energy redirection" to generate control forces with increased fidelity while remaining dissipative and safe. Experimental validation of the method, for complete pose control, shows that it achieves a 90% reduction in task error compared with the current state of the art in dissipative control for the tested applications. The findings clearly demonstrate that the method significantly increases the fidelity and efficacy of dissipative control during physical human–robot interaction. This advancement expands the number of tasks and environments into which safe physical human–robot interaction can be employed effectively.

Index Terms—Haptics and haptic interfaces, impedance control, medical robots and systems, physical human–robot interaction, virtual fixtures.

I. INTRODUCTION

A. Motivation

FROM surgery to car assembly, robotic systems have been applied to a wide range of applications, where they cooperate with humans via a direct physical interaction [1], [2]. Robots offer many attributes in such a collaboration, including accuracy, precision, integration with external devices and sensing, and untiring strength. At present, however, robotic systems are often inferior to their human counterparts in terms of their cognition of the operating environment and task, particularly when they are unstructured. Physical human–robot interaction provides a method for combining human and robot competencies effectively [3].

During physical human–robot interaction, there are several benefits to ensuring that the robotic part of the system is

energetically dissipative. This means that the robot does not generate any energy within the interaction and only stores a bounded amount of energy supplied to it by the user [4], [5]. The dissipative robot will not start moving without initiation from the user, will not make sudden discontinuous jumps during movement, and will come to a halt once the user stops interacting with it. Due to the requirement for external energy input, a dissipative robot typically has reduced fidelity and less control over its pose than a conventional "active" robot; however, there are many occasions in which it is favorable to ensure smooth, regulated, and safe movements in the presence of potentially error-prone robot perception.

Dissipative control in physical human–robot interaction is particularly advantageous for active constraints/virtual fixtures [6], [7] in robot-assisted surgery. In this method, a robot regulates the motion of cooperatively controlled surgical instruments to improve outcomes in procedures such as sinus [8] and knee replacement [9] surgery. In the most commercially successful surgical robots, for example, the da Vinci surgical system (Intuitive Surgical Inc.) and RIO (Mako Surgical Corp.), ultimate control of the procedure resides with the surgeon. These systems operate as "intelligent tools" [10], assisting with features such as haptic guidance or motion scaling. They are not required or wanted to make procedural decisions of their own, matching dissipative control's attributes.

B. Related Work

Safety during physical human–robot interaction has been widely researched [11]. Collision characteristics have been improved by reducing manipulator dynamic masses [12], incorporating series elastic actuators [13], and using impedance or force control [14]. The general limitation of these approaches is that they are primarily concerned with the safety of the human operator, stopping a robot before it applies harmful levels of force to users. In this study, preventing small erroneous forces and motions that can have a severe impact on task performance is an important consideration. Ensuring a robot is dissipative guarantees both task and user safety.

Several robots for physical human–robot interaction have been developed with custom dissipative mechanisms. Collaborative robot (COBOT) controls gear ratios in continuously variable transmissions to restrict end-effector motion [2], passive arm with dynamic constraints (PADyC) achieves a similar effect with contra-rotating freewheels and clutches [15], as does the passive trajectory enhancing robot (P-TER) with clutches and brakes [16]. In addition to requiring custom hardware, controlling all degrees of freedom can be impossible in such systems or requires the use of complicated and cumbersome mechanisms.

To overcome these issues, it is possible to control conventional, motor based, robots to exhibit similar energetic characteristics.

Dissipative control of a conventional robot has been implemented with an anisotropic friction model in "non-energy-storing virtual fixtures" [17]. They apply a frictional resistance when moving in a restricted direction, and little or no resistance when moving in a permitted direction. This method was shown to be effective at guiding the user; however, the fidelity of the haptic information which can be communicated by a pure friction model of this form is limited. The primary issue is that, as shown in Fig. 1(a) and (b), friction only generates forces antiparallel to a component of motion. The resulting lack of haptic communication can reduce the controller's effectiveness and, subsequently, the task's accuracy.

There are many other techniques for augmenting performance during physical human–robot interaction, typically under the name virtual fixtures or active constraints. However, the majority of methods involve some degree of energetic activity, such as viscoelastic control [18], potential fields [19], and joint optimization [8]. The only notable exceptions are non-energy-storing continuous impulsive forces [20], although they require reinforcement with an active controller to achieve good steady-state performance and "reference direction fixtures" [21], the inspiration for the energy redirection concept, which requires admittance controlled robots. Neither of which considers the link between translation and rotation.

C. Research Contributions

In this paper, a novel dissipative controller for physical human–robot interaction is described and validated. This controller addresses the central challenge of reduced fidelity in dissipative control to provide increased efficacy in robotic assistance, expanding the number of tasks and environments in which the uniquely safe form of control is able to provide significant benefit, both extending existing applications and enabling new ones. The advancement to dissipative control is provided by employing a novel unified consideration of energy during multidimensional human–robot interaction and a technique termed "energy redirection." Energy redirection allows the controller to take energy from the user in one dimension and reintroduce it in another by applying friction at an oblique angle to the direction in which force is required. This concept is illustrated in Fig. 1(c) and (d).

In preliminary studies [22], [23], energy redirection was posited by the authors and explored in simplified manipulation tasks, under the name "dynamic frictional constraints." In [22], the concept was found to be effective in dynamic position guidance, although not as much as an (energetically active) proportional-derivative controller. In [23], the mathematical formulation for the controller was consolidated, proven to be dissipative and extended to operate in position and orientation. However, the initial research only considered energy redirection between isotropic dimensions (i.e., with single units for displacement). In this study, in addition to thorough theoretical and experimental analyses, the complete unified dissipative controller is presented that can simultaneously control tasks in any anisotropic dimensions (i.e., with different units for dis-
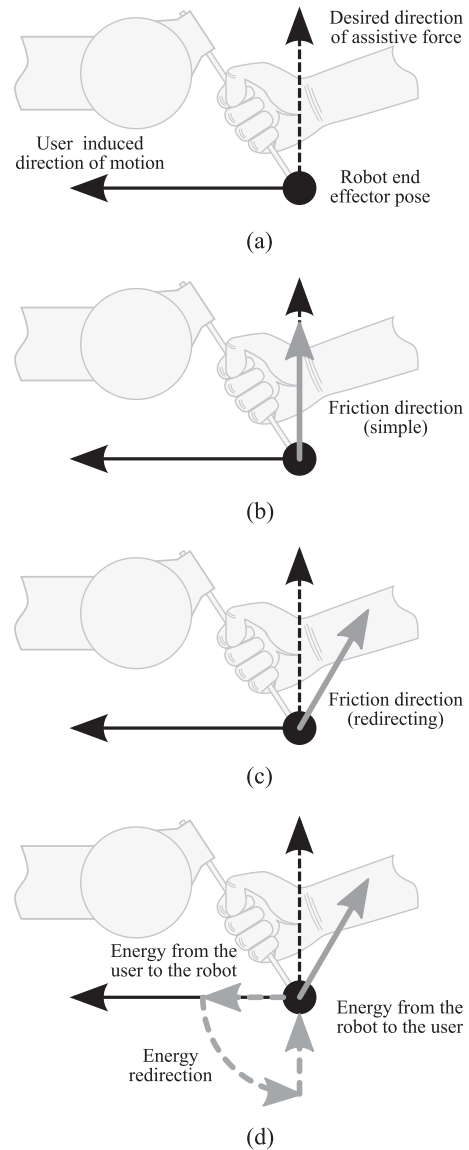

Fig. 1. Illustration of a simple friction based controller and how energy redirection can supply richer feedback for the user. (a) In this scenario, the desired direction of assistive force is orthogonal to the current direction of motion. (b) Aligning the friction direction with the desired motion/force direction will not generate assistive forces due to their orthogonality. (c) This can be overcome by setting the friction direction oblique to the desired direction of force. (d) The oblique angle of the friction allows the users' energy applied in the direction of motion to be redirected by the controller and applied in the direction in which an assistive force is required.

placement), as are found in almost all practical manipulation tasks. This crucial final element of the controller makes it more efficient with the energy provided by the user. The complete consideration of energy allows a controller to generate much more haptic information than would otherwise be possible, thus providing greater user assistance while remaining dissipative. In addition, this paper also contains the first published experimental investigation into the effectiveness of haptic assistance (active constraints/virtual fixtures) in dynamic soft-tissue dissection tasks. Applying the dissipative controller to protect soft tissue structures in a surgical simulation, extensive experimentation
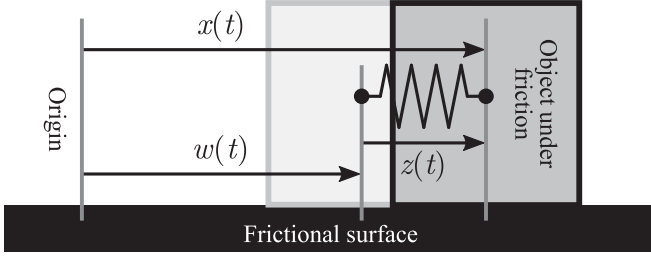
Fig. 2. Illustration of the elastoplastic friction model created by Dupont *et al.* [24]. The object's total displacement $x(t)$ is the sum of the plastic $w(t)$ (i.e., permanent) and elastic $z(t)$ (i.e., reversible) components.

quantifies the benefit that such augmentation can provide over unassisted surgery.

II. DISSIPATIVE CONTROL IN n-DIMENSIONS

In Section II-A, the elastoplastic friction model is revised from [23], and in Section II-B, the energy redirection method and n-dimensional dissipative formulation are presented.

A. Elastoplastic Friction in n-Dimensions

1) Elastoplastic Friction Model: Friction is a naturally dissipative mechanic, as its forces always resist motion. Although there are a range of ways to model friction, the "elastoplastic friction model" [24] is widely used. The formulation is similar to the well-established Dahl [25] and LuGre [26] models; however, it prevents "nonphysical drift" by including a purely elastic presliding component.

In the elastoplastic friction model (see Fig. 2), an object's displacement $x(t)$ is comprised of a permanent, plastic component $w(t)$, and a reversible elastic component $z(t)$. The elastic displacement represents the physical phenomenon of presliding, considered in the LuGre model as deflections in microscopic bristles between the contacting surfaces. The elastic presliding displacement is the model's internal state variable, from which the friction force $f_f(t)$ is computed [24] as

$$f_f(t) = \sigma_0 z(t) + \sigma_1 \dot{z}(t) + \sigma_2 \dot{x}(t) \tag{1}$$

where σ_0, σ_1, and σ_2 are the stiffness, tangential compliance damping, and viscous friction coefficients, respectively.

From an initial value, the elastic presliding state variable, $z(t)$, changes as defined in the following equation, from [24]:

$$\dot{z}(t) = \dot{x}(t) \left(1 - \alpha(z, \dot{x}) \frac{z(t)}{z_{ss}(\dot{x})} \right) \tag{2}$$

where α defines the displacement type (elastic: $\alpha = 0$, plastic: $\alpha = 1$ or mixed: $0 < \alpha < 1$) and z_{ss} is the steady-state elastic displacement (i.e., the maximum magnitude of z).

A discretization of the elastoplastic friction model is described in [27], which uses the Euler method to discretize (2) and formulate it into two saturation operations that can be implemented computationally. It was shown in [23] that, to represent Coulomb friction, the discrete elastoplastic friction model can

be simplified into a single expression as

$$z_k = \begin{cases} z_c, & |z_c| < z_{css} \\ z_{css}, & z_c \geq z_{css} \\ -z_{css}, & z_c \leq -z_{css} \end{cases} \tag{3}$$

where $z_k \in \mathbb{R}$ is the elastic presliding displacement at time step k, $z_c \in \mathbb{R}$ is the candidate z_k value assuming a purely elastic displacement, and $z_{css} \in \mathbb{R}$ is the Coulomb friction steady-state elastic displacement value

$$z_c = z_{k-1} + \Delta x_k \tag{4}$$

$$z_{css} = f_C / \sigma_0 \tag{5}$$

where $z_{k-1} \in \mathbb{R}$ is the elastic presliding displacement at the previous time step, $x_k \in \mathbb{R}$ is the object's displacement at time step k, and $f_C \in \mathbb{R}$ is the Coulomb friction force.

In (3), the elastic displacement is computed by first calculating the purely elastic candidate displacement, z_c, then clamping it between $\pm z_{css}$, i.e., by applying the following projection operation to z_c into C_{ep}:

$$z_k = \underset{w \in C_{ep}}{\arg \min} \|w - z_c\| \tag{6}$$

where $C_{ep} \subset \mathbb{R}$ is the set of real displacements with absolute values less than the Coulomb friction steady-state elastic displacement

$$C_{ep} = \{ w : w \in \mathbb{R}, |w| \leq z_{css} \}. \tag{7}$$

The computation of the elastic displacement is presented as a projection of the candidate elastic displacement into a subset of the Cartesian space, as this concept is fundamental to the dissipative controller presented below.

2) n-Dimensional Formulation: With n-dimensional vectors, the expression for computing the friction force within the simplified elastoplastic friction model becomes

$$\mathbf{f}_{f,k} = \Sigma_0 \mathbf{z}_k + \Sigma_1 \dot{\mathbf{z}}_k + \Sigma_2 \dot{\mathbf{x}}_k \tag{8}$$

where $\mathbf{f}_{f,k} \in \mathbb{R}^n$ is the friction force/torque at time step k, $\mathbf{z}_k \in \mathbb{R}^n$ is the elastic presliding displacement at time k, $\mathbf{x}_k \in \mathbb{R}^n$ is the total displacement at time step k, and $\Sigma_0, \Sigma_1, \Sigma_2 \in \mathbb{R}^{n \times n}$ are the three diagonal gain matrices defined as

$$\Sigma_0 = \operatorname{diag}(\sigma_{0,1}, \sigma_{0,2}, \ldots, \sigma_{0,n}) \tag{9}$$

$$\Sigma_1 = \operatorname{diag}(\sigma_{1,1}, \sigma_{1,2}, \ldots, \sigma_{1,n}) \tag{10}$$

$$\Sigma_2 = \operatorname{diag}(\sigma_{2,1}, \sigma_{2,2}, \ldots, \sigma_{2,n}) \tag{11}$$

where the elements of the diagonals correspond to the values for friction coefficients $\sigma_0, \sigma_1, \sigma_2$ in each of the n dimensions.

To apply elastoplastic friction in n-dimensional space, the equivalent to the 1-D projection of the candidate elastic displacement in (6) is a projection of the candidate elastic displacement into an $(n-1)$-ellipse. Formally, it is calculated from

$$\mathbf{z}_k = \underset{\mathbf{w} \in C_{epn}}{\arg \min} \|\mathbf{w} - \mathbf{z}_c\| \tag{12}$$

where $\mathbf{z}_c \in \mathbb{R}^n$ is the candidate for $\mathbf{z}_k$, assuming a purely elastic displacement, at time k, and $C_{epn} \subset \mathbb{R}^n$ is the set of

displacements with magnitudes less than the Coulomb friction steady-state elastic displacement

$$C_{\mathrm{epn}} = \{\mathbf{w} : \mathbf{w} \in \mathbb{R}^n, ||\mathbf{w}|| \leq Z_{\mathrm{css}}(\mathbf{w})\} \qquad (13)$$

where $Z_{\mathrm{css}}(\cdot) : \mathbb{R}^n \to \mathbb{R}$ is a function that computes the Coulomb friction steady-state displacement in the given direction, equivalent to (5), as

$$Z_{\mathrm{css}}(\mathbf{w}) = F_{\mathrm{c}}(\mathbf{w})/\Sigma_0(\mathbf{w}) \qquad (14)$$

where $F_c(\cdot) : \mathbb{R}^n \to \mathbb{R}$ is a hardware/application specific function which computes the Coulomb friction force in a given direction and $\Sigma_0(\cdot) : \mathbb{R}^n \to \mathbb{R}$ is a function which computes the friction stiffness in a given direction, as

$$\Sigma_0(\mathbf{w}) = \frac{||\Sigma_0 \mathbf{w}||}{||\mathbf{w}||}. \qquad (15)$$

The reason for projecting the candidate elastic displacement into an $(n-1)$-ellipse with variable radius $Z_{\mathrm{css}}(\cdot)$, rather than an $(n-1)$-sphere with constant radius z_{css}, is that there is often dimensional anisotropy within the robotic hardware and the desired friction properties, i.e., the required Coulomb friction force $F_c(\cdot)$ and the required frictional stiffness $\Sigma_0(\cdot)$ are different in different dimensions. If these values change between dimensions, then the steady-state Coulomb friction displacement also changes between dimensions. In practice, $F_c(\cdot)$ and $\Sigma_0(\cdot)$ are dependent on the robotic hardware's manipulability ellipsoid [28], or a simplification of it.

Unlike in the simple scalar case, in the generalized case, displacements are not necessarily linear (for example, if one component of the displacement is a rotation). To account for this, the candidate elastic displacement vector, $\mathbf{z}_k$, is defined as

$$\mathbf{z}_c = \mathbf{z}_{k-1} \oplus \Delta\mathbf{x}_k \qquad (16)$$

where $\mathbf{z}_{k-1} \in \mathbb{R}^n$ is the elastic presliding displacement at the previous time step, $\mathbf{x}_k \in \mathbb{R}^n$ is the object's displacement at time step k, and $\oplus$ is an abstract addition operator symbolizing the vector addition necessary for the displacement types.

B. Energy Redirection via Conical Projections

1) Energy Redirection Concept: Implementing the friction model above as an impedance controller on a robot, with necessary dynamic compensation for the robot itself, generates forces at the end effector that discretely approximate Coulomb friction. The model's forces oppose motion in any direction, translation, or rotation. To control a robot's pose using a dissipative impedance controller such as this, it is necessary to increase the anisotropy in the Coulomb friction such that it "encourages" user motion toward the desired pose and "discourages" user motion away from the desired pose.

Previously, Kikuuwe *et al.* used friction to discourage motion away from a robot's desired pose by enforcing friction along the desired direction of motion [17]. This is approximately equivalent to the illustration in Fig. 1(b). This prevented the user from moving away from the desired pose; however, it was not able to encourage the user to move towards to the desired pose. In [22], the proposed solution to this issue was to vary the friction
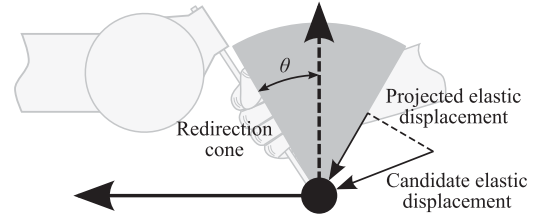

Fig. 3. Illustration of the conical projection concept for energy redirection. The redirection cone with apex angle θ is aligned with the direction of the desired motion and the candidate elastic displacement is projected onto it to form the elastic displacement used in the friction model.

direction based on the direction of motion. When the robot was moving directly away from the desired pose, the friction model would be aligned in the same way as [17], resisting further motion. When the robot was moving directly toward the desired pose, the friction model would allow the user to move freely. The novelty of this approach was when the user was moving orthogonally to the desired direction of motion. In this case, the friction model was applied obliquely to the desired direction of motion, as illustrated in Fig. 1(c), generating frictional forces that control the robot toward the desired pose.

In [23], the oblique frictional forces were formulated in terms of the energy transferred between the robot and user. As illustrated in Fig. 1(d), the oblique friction takes energy from the user in the orthogonal direction of motion and reapplies it to the user to control the pose, while remaining dissipative. The method proposed for enforcing oblique friction using the elastoplastic model was projecting the candidate elastic displacement vector into a cone (generating friction forces in only certain directions of movement) rather than an ellipse (generating friction forces in all directions of movement).

By aligning the redirection cone with the direction of desired motion (see Fig. 3), the projection ensures that the elastic displacement within the friction model and therefore also the quasi-static friction force are approximately in that direction. Varying the angle θ balances the energy transferred between dimensions and controls the controller's forcefulness. Smaller angles redirect less energy and control the pose less strongly; however, larger angles can inhibit orthogonal motion.

This conical projection transfers energy between dimensions such that, even if the user moves orthogonally to the desired direction of force, a control force is generated. When the user moves orthogonally to the desired direction of force, the projected elastic displacement migrates along the edge of the cone, generating a friction force in that direction. The projection operation takes user provided energy in the horizontal direction and stores some of this energy in the vertical component of the elastic displacement, thus allowing it to transfer energy back to the user in a different dimension.

The use of conical projections of the elastic displacement within the elastoplastic friction model was proposed and validated for translation and rotation control, independently of one another, in [23]. The challenge with the given friction formation and control approach is when the dimensions have different units for displacements (i.e., meters, radians, etc.) or different

implementable stiffnesses (i.e., values for σ_0). This anisotropy means that, if the projection of the candidate elastic displacement $\mathbf{z}_c$ is performed as shown in (12), then it could increase the potential energy within the system, violating the dissipative control requirement. To understand this behavior, the potential energy function $P(\cdot) : \mathbb{R}^n \to \mathbb{R}$ is introduced, which computes the total elastic potential energy stored within the elastic displacement of the friction model

$$P(\mathbf{a}) = \frac{1}{2} \mathbf{a} \cdot \Sigma_0 \mathbf{a} \tag{17}$$

where $\mathbf{a} \in \mathbb{R}^n$ is an arbitrary multidimensional elastic displacement vector.

Projecting the candidate elastic displacement vector into either an ellipse or a cone will not increase the magnitude of the elastic displacement vector (i.e. $\|\mathbf{z}_k\| \leq \|\mathbf{z}_c\|$); however, if there is dimensional anisotropy in the stiffness values σ_0, then the potential energy in the elastic displacement may increase as

$$\|\mathbf{z}_k\| \leq \|\mathbf{z}_c\| \not\Rightarrow P(\mathbf{z}_k) \leq P(\mathbf{z}_c). \tag{18}$$

It was for this reason that the 6-D formulation presented in [23] considered translation and rotation independently of one another. In the following sections, it is explained how the projection operation can be generalized to operate simultaneously in arbitrary anisotropic dimensions.

2) Combining Anisotropic Dimensions: The solution to dimensional anisotropy during the conical projection is to represent elastic displacements $\mathbf{z}_k$ and candidate elastic displacements $\mathbf{z}_c$ in terms of the elastic potential energies stored within their representative springs. By projecting potential energy, instead of displacement, the dimensions become isotropic and it is guaranteed that the potential energy stored will not increase, and the system will remain dissipative.

To apply projections to potential energies, rather than spring displacements, it is necessary to map the vectors into the "potential energy space." The potential energy mapping $M : \mathbb{R}^n \to \mathbb{R}^n$ is defined as

$$M(\mathbf{a}) = \tilde{\mathbf{a}} \tag{19}$$

such that

$$\tilde{\mathbf{a}}_i = \mathrm{sgn}(\mathbf{a}_i)\sqrt{P(\mathbf{a}_i)} = \mathrm{sgn}(\mathbf{a}_i)\sqrt{\frac{1}{2} \Sigma_{0,i} \mathbf{a}_i^2} \tag{20}$$

where $i = [1, n]$, $\mathbf{a}_i \in \mathbb{R}$ is the ith element of the input vector $\mathbf{a} \in \mathbb{R}^n$, $\tilde{\mathbf{a}}_i \in \mathbb{R}$ is the ith element of the output vector $\tilde{\mathbf{a}} \in \mathbb{R}^n$, and $\Sigma_{0,i} \in \mathbb{R}$ is the ith element along the diagonal of the stiffness matrix Σ_0. The inverse of the potential energy mapping $M^{-1} : \mathbb{R}^n \to \mathbb{R}^n$ is similarly defined as

$$M^{-1}(\tilde{\mathbf{a}}) = \mathbf{a} \tag{21}$$

such that

$$\mathbf{a}_i = \mathrm{sgn}(\tilde{\mathbf{a}}_i)\sqrt{\frac{2\tilde{\mathbf{a}}_i^2}{\Sigma_{0,i}}}. \tag{22}$$

Once the potential energy mapping has been applied to an elastic displacement vector, the ith element within the output vector represents the square root of the elastic potential energy stored in the ith dimension of $\mathbb{R}^n$.

3) Conical Projections in the Potential Energy Space: To apply the controller at each time step, the candidate elastic displacement and desired motion direction must be mapped into the potential energy space. Here, the energy redirecting conical projection is applied, before the resulting elastic displacement is mapped back into Cartesian space and used in the friction model in (8).

Similarly to the n-ellipse projection for generating elasto-plastic friction in all directions in (12), the conical projection for applying dissipative control within the potential energy space is defined as

$$\tilde{\mathbf{z}}_k = \arg\min_{\mathbf{w} \in \tilde{C}_k} \|\mathbf{w} - \tilde{\mathbf{z}}_c\| \tag{23}$$

where $\tilde{\mathbf{z}}_k = M(\mathbf{z}_k)$, $\tilde{\mathbf{z}}_c = M(\mathbf{z}_c)$, and $\tilde{C}_k \subset \mathbb{R}^n$ is the closed conical set aligned with the desired direction of force $\tilde{\mathbf{p}}_k$, defined as

$$\tilde{C}_k = \left\{ \mathbf{w} : \mathbf{w} \in \mathbb{R}^n, \|\mathbf{w}\| \leq \tilde{Z}_{\mathrm{css}}(\mathbf{w}), \Theta(\mathbf{w}, \tilde{\mathbf{p}}_k) \leq \theta \right\} \tag{24}$$

where $\Theta(\cdot, \cdot) : \mathbb{R}^n \times \mathbb{R}^n \to \mathbb{R}$ is a binary function computing the angle between two vectors, $\tilde{\mathbf{p}}_k \in \mathbb{R}^n$ is the potential energy mapped desired direction of force, $\tilde{\mathbf{p}}_k = M(\mathbf{p}_k)$, and $\tilde{Z}_{\mathrm{css}}(\cdot) : \mathbb{R}^n \to \mathbb{R}$ is a function which computes the Coulomb friction steady-state displacement in the given direction of the potential energy space, defined as

$$\tilde{Z}_{\mathrm{css}}(\mathbf{w}) = \left\| M \left(Z_{\mathrm{css}}(M^{-1}(\mathbf{w})) \frac{M^{-1}(\mathbf{w})}{\|M^{-1}(\mathbf{w})\|} \right) \right\|. \tag{25}$$

As the change in $\mathbf{z}_k$ at each time step is small, the conical projection described in the two previous equations can be approximated using the following closed-form expression:

$$\tilde{\mathbf{z}}_k = \begin{cases} \tilde{\mathbf{z}}_c, & \Theta(\tilde{\mathbf{z}}_c, \tilde{\mathbf{p}}_k) \leq \theta \wedge \|\tilde{\mathbf{z}}_c\| \leq \tilde{Z}_{\mathrm{css}}(\tilde{\mathbf{z}}_c) \\ \tilde{Z}_{\mathrm{css}}(\tilde{\mathbf{z}}_c)\dfrac{\tilde{\mathbf{z}}_c}{\|\tilde{\mathbf{z}}_c\|}, & \Theta(\tilde{\mathbf{z}}_c, \tilde{\mathbf{p}}_k) \leq \theta \wedge \|\tilde{\mathbf{z}}_c\| > \tilde{Z}_{\mathrm{css}}(\tilde{\mathbf{z}}_c) \\ \tilde{y}_c \hat{\mathbf{y}}, & \text{otherwise} \end{cases} \tag{26}$$

where $\hat{\mathbf{y}} \in \mathbb{R}^n$ is a unit vector defining the edge of the cone $\tilde{C}_k$ on the hyperplane through $\tilde{\mathbf{z}}_c$ and $\tilde{\mathbf{p}}_k$, and $\tilde{y}_c \in \mathbb{R}$ is the scalar projection of $\tilde{\mathbf{z}}_c$ onto $\hat{\mathbf{y}}$, clamped between 0 and $\tilde{Z}_{\mathrm{css}}(\hat{\mathbf{y}})$, as

$$\tilde{y}_c = \begin{cases} 0, & \tilde{\mathbf{z}}_c \cdot \hat{\mathbf{y}} \leq 0 \\ \tilde{\mathbf{z}}_c \cdot \hat{\mathbf{y}}, & 0 < \tilde{\mathbf{z}}_c \cdot \hat{\mathbf{y}} < \tilde{Z}_{\mathrm{css}}(\hat{\mathbf{y}}) \\ \tilde{Z}_{\mathrm{css}}(\hat{\mathbf{y}}), & \text{otherwise.} \end{cases} \tag{27}$$

In the Appendix, it is proven that this discrete control formulation conforms to the formal definition of energetic dissipativity and therefore ensures that the human user retains primary control of the motion of the robotic system.

It is well established that the energy storage function for a dissipative dynamical system is a valid Lyapunov function candidate, and under certain assumptions that are met by the proposed controller, it can be used to prove stability [5], [29]. In much the same way that the passivity of a subsystem within

a two-port network can be used to demonstrate the stability of a complete system [30], proving the dissipativity of a subsystem can prove overall stability [31]. This modular consideration of stability analysis is vital for physical human–robot interaction, because the dynamic properties of the human cannot be reliably modeled. Consequently, proving that the control strategy is dissipative is sufficient to ensure stability for the complete system under the assumptions that the robot force/torque controller is passive, and the human arm acts passively at the frequencies of interest for stability [32]. The disconnected approach means that the convergence of the controller cannot be quantified analytically; therefore, proof of this is demonstrated empirically in the following sections.

4) Concrete Implementations in Position and Orientation: Presenting the dissipative controller in a generalized n-dimensional form means that it can be applied to a range of different task-space configurations involving position and/or orientation. If control is required on position, then elements of the displacement vector $\mathbf{x}_k$ should be defined as linear translational displacements in the required Euclidean space, i.e., $\mathbb{R}^1$, $\mathbb{R}^2$, $\mathbb{R}^3$, etc. If control is required on orientation, then elements of the displacement vector $\mathbf{x}_k$ should be defined as the rotation vector linearization of the special orthogonal group of rotations, i.e., SO(1), SO(2), SO(3), etc. As explained in detail in [23], using rotation vector representations of orientation ensures the correctness of the energy redirection.

Any required combination of position and orientation control can be achieved using the controller by simply concatenating their respective vector descriptions into one. For example, to control position and orientation within the special Euclidean group in three dimensions, SE(3), each of the components within the friction model should be defined in $\mathbb{R}^6$ as

$$\mathbf{x}_k = [\mathbf{x}_{t,k}, \quad \mathbf{x}_{r,k}] \tag{28}$$

where $\mathbf{x}_{t,k} \in \mathbb{R}^3$ is the translational displacement, and $\mathbf{x}_{r,k} \in \mathbb{R}^3$ is the rotational displacement in SO(3), represented as a rotation vector.

III. Experimental Validation

Two sets of experiments were performed to validate the proposed dissipative control. The first experiment was used for a statistically robust analysis of the abstracted properties of the controller. The second experiment was based on the application of the method to a practical task and investigated the controller's efficacy in a more complete scenario.

Both experiments were implemented in C++ using the Open Robot Control Software (OROCOS) [33] through Linux, with a 3.0-GHz Core i7 CPU (Intel, Corp.). The haptic device control rates were set at 1 kHz. The visualizations for all experiments were run on a separate PC, through Windows (Microsoft Corp.), with a 2.93-GHz Core i7 CPU (Intel, Corp.)/Quadro 4000 GPU (NVIDIA Corp.). To aid with users' depth perception in the simulated environments, the visualizations were presented to the users on a 3-D monitor using NVIDIA 3D Vision (NVIDIA Corp.). The communication between the control and visualiza-
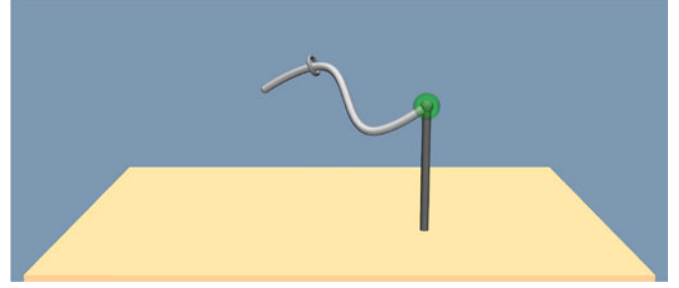

Fig. 4. Visualization from the simulated steady-hand game. Shown is the deforming wire pathway, the user-controlled ring, and the active target position.

tion PCs was via the user datagram protocol (UDP) at approximately 40 Hz.

The controller proposed in this paper can be used to control the pose of a range of robots that are directly manipulated by a human user. To allow accurate quantification of task performance, a telemanipulation scenario was simulated, in which the user interacts with a master haptic device. Dissipative control was applied directly at the master device, and the slave robot was simulated to perfectly follow the master.

A. Steady-Hand Game

The proposed control scheme was initially validated with a simulation of the *The Steady-Hand Game*, as was used in the concept validation in [23]. In the steady-hand game, a user attempts to move a ring along a wire pathway, while preventing the wire and ring from making contact with one another. This game was selected for validating the controller because it requires precise and dexterous manipulation from the human user simultaneously in multiple degrees of freedom.

The steady-hand game simulation is shown in Fig. 4. The user controlled the pose of the ring with a six degree of freedom, sigma.6+ haptic device (Force Dimension Inc.), which also rendered control forces/torques to the user. Dynamism was introduced into the task by randomly deforming the wire at approximately 12 mm.s^{-1}, the ring's inner diameter was 14 mm, and the wire pathway's diameter was 8 mm.

Six control methods were applied to assist the users. The methods are explained below, with the displacement representations described in terms of Cartesian translations t_x, t_y, t_z and rotations r_x, r_y, r_z. The redirection cone apex angle θ controls the friction direction when the robot moves orthogonal to the desired direction of motion.

1) **NC** no control, unassisted.
2) **DC3T** 3-D dissipative control in translation, where $\mathbf{x}_k = [t_x, t_y, t_z, 0, 0, 0]$ and $\theta = 30°$.
3) **DC3R** 3-D dissipative control in rotation, where $\mathbf{x}_k = [0, 0, 0, r_x, r_y, r_z]$ and $\theta = 30°$.
4) **DC6U** 6-D dissipative control with translation and rotation uncoupled from one another, i.e., simultaneous independent application of DC3T and DC3R.
5) **FC6** 6-D dissipative control in translation and rotation, where $\mathbf{x}_k = [t_x, t_y, t_z, r_x, r_y, r_z]$ and $\theta = 0°$.
6) **DC6** full 6-D dissipative control in translation and rotation, where $\mathbf{x}_k = [t_x, t_y, t_z, r_x, r_y, r_z]$ and $\theta = 30°$.

TABLE I
PARAMETERS FOR THE DISSIPATIVE CONTROLLER IN THE STEADY-HAND GAME
EXPERIMENTS

Parameter	Value
f_C	15.0 N
τ_C	400.0 N.mm
Σ_0	$\mathrm{diag}(2, 2, 2, 1600, 1600, 1600)$
Σ_1	$\mathrm{diag}(0, 0, 0, 0, 0, 0)$
Σ_2	$\mathrm{diag}(0.007, 0.007, 0.007, 60, 60, 60)$

For cases where fewer than six dimensions were controlled, the parameters for the uncontrolled dimensions were set to zero.

Method FC6 was the primary comparison state-of-the-art method, functionally similar to [17], without energy redirection between dimensions. Unlike in [22], no comparison was made with an energetically active controller because, with the high force and stiffness capabilities of the haptic device, negligible violation would occur in the simulated environment.

The desired direction of motion $\mathbf{p}_k$ was computed as the vector from the current tool pose to the closest point on the pathway's centerline with the ring's axis tangent to the pathway. The parameters used in the controller are shown in Table I. These values were set based on the capabilities of the sigma.6+ and the section of its workspace in use. The Coulomb friction function F_c used in (14) was set as

$$F_c(\mathbf{w}) = \begin{cases} f_C, & \dfrac{\|H\Sigma_0\mathbf{w}\|}{f_C} \geq \dfrac{\|T\Sigma_0\mathbf{w}\|}{\tau_C} \\ \tau_C, & \text{otherwise} \end{cases} \quad (29)$$

where $H \in \mathbb{R}^{6\times 6}$ and $T \in \mathbb{R}^{6\times 6}$ are diagonal matrices selecting the three head and tail elements, respectively, of a vector

$$H = \mathrm{diag}(1, 1, 1, 0, 0, 0) \quad (30)$$

$$T = \mathrm{diag}(0, 0, 0, 1, 1, 1). \quad (31)$$

After reading the instructions, and a period of familiarization, 20 users took part in the experiments. This consisted of 17 males/3 females and 18 right/2 left handed people, with an age range of 22–38. There was a total of 30 tests per subject with multiple randomized pathway geometries.

B. Soft Tissue Dissection

To investigate the efficacy of the controller in a more encompassing practical task, a simulation of robot-assisted clinical dissection, inspired by the da Vinci Surgical System, was used. The selected scenario was the dissection of a tubular tissue structure, such as a nerve or vessel, embedded within a larger mass of soft tissue, shown in Fig. 5(a). A simulated environment was used in place of a physical teleoperated robot because it allowed a quantitative analysis of performance and simplified the anatomical tracking. It was posited that the surgeon wanted to avoid causing damage to the tubular structure by cutting or crushing it, and therefore, the controllers, within the framework of an active constraint/virtual fixture, were applied to prevent the scalpel from intersecting it.
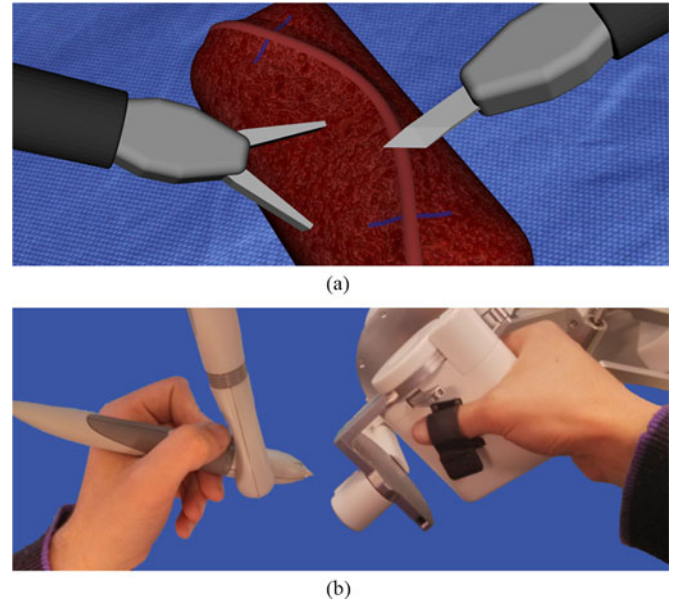

Fig. 5. Alignment of the master haptic devices with the simulated surgical instruments. The left-hand haptic device, the Phantom Omni, controlled the forceps, and the right-hand device, the sigma.6+, controlled the scalpel. (a) Simulated surgical instruments. (b) Master haptic devices.

The complete system for the experiment is shown in Fig. 6. Descriptions of the individual components follow.

1) Active Constraint Controller: The implementation of the dissipative controller within the experiment was in the framework of an active constraint controller, as defined in [6]. In order for a desired direction of motion $\mathbf{p}_k$ to be input, at each time step in the simulation, a target pose was computed for the scalpel blade which avoided penetrating the tubular structure. This target pose was defined with the use of a six-degree-of-freedom dynamic proxy, adapted from the constraint-based method in [34]. To identify potential contacts between the scalpel proxy (a single quadrilateral) and the tubular structure (a triangular mesh), a deformation invariant bounding sphere hierarchy [35] was used that efficiently evaluated proximity queries at well above the 1-kHz requirement.

The parameters used in the controller are shown in Table II and the Coulomb friction function F_c was the same as that used in (29).

2) Physical Soft Tissue Simulation: To simulate realistic soft tissue interactions between the surgical instruments and the soft tissue, a mechanical simulation was constructed using the Simulation Open Framework Architecture (SOFA) [36]. The tissue block and tubular structure were both modeled using custom tetrahedral meshes, and their deformations were solved using the large strain linear finite element method with an implicit conjugate-gradient based solver, all of which were available in SOFA. The simulation rate for each time step was approximately 20–200 Hz depending on the deformation of the models and the number of contacts.

3) Hardware Interface: A Phantom Omni haptic device (Sensable Technologies, Inc.) and a sigma.6+ haptic device were used as the master devices within the simulation system to control the forceps and scalpel, respectively. The alignment of the
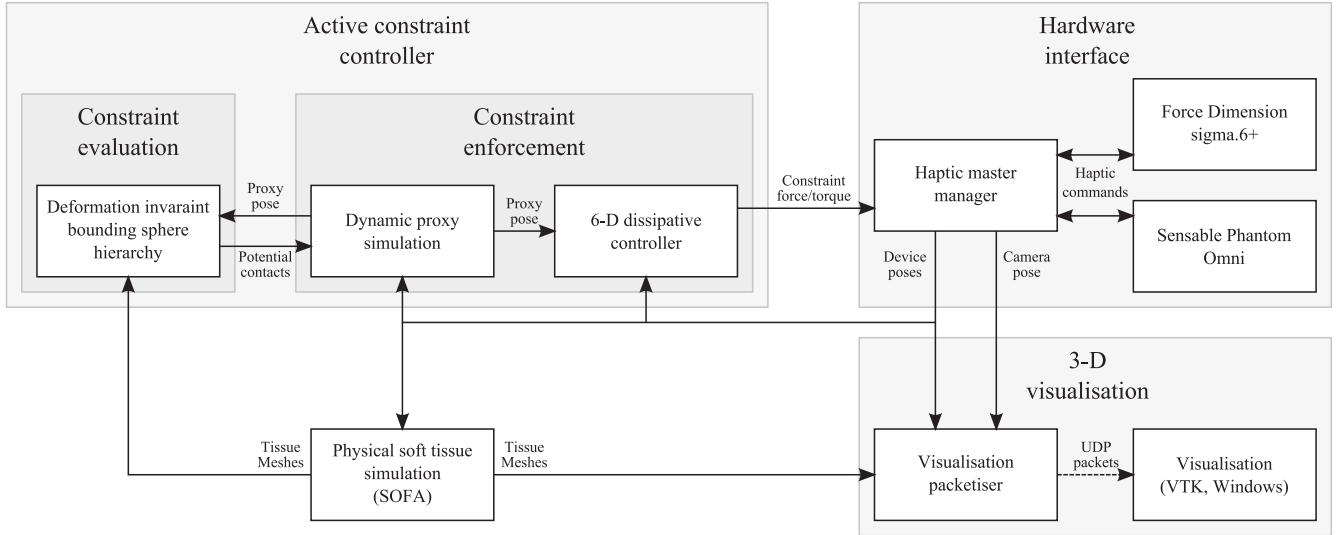
Fig. 6.   System diagram for the software used within the simulated surgical environment.

TABLE II
PARAMETERS FOR THE DISSIPATIVE CONTROLLER IN THE SOFT TISSUE
DISSECTION EXPERIMENTS

Parameter	Value
f_C	15.0 N
τ_C	500.0 N.mm
Σ_0	$\mathrm{diag}(3, 3, 3, 2000, 2000, 2000)$
Σ_1	$\mathrm{diag}(0, 0, 0, 0, 0, 0)$
Σ_2	$\mathrm{diag}(0.007, 0.007, 0.007, 20, 20, 20)$

These are defined in the Cartesian space of the master device, and not the simulated environment after motion scaling. For cases where fewer than six dimensions were controlled, the parameters for the uncontrolled dimensions were set to zero.

haptic devices to the simulation is shown in Fig. 5. For the dissection task, a motion scaling value of 5:1 was implemented in translation, based on the da Vinci surgical system. The active constraints were applied based on the Cartesian motion of the master device, and not the scaled motion of the simulated slave. It is possible to apply dissipative control at the slave side of an anisotropically scaled Cartesian space; however, this will be formalized in future work.

4) Three-Dimensional Visualization: To display the simulation to the user, a 3-D visualization of the surgical scene was constructed using the Visualization ToolKit (VTK, Kitware, Inc.) and rendered at 40 Hz, as shown in Fig. 5(a).

5) Experimental Procedure: Several users performed repeated dissections of the tubular structure from the tissue block, while the dissipative controllers provided assistance to them. In each test, a user dissected the structure from the tissue block, in the area between the two blue marks, as shown in Fig. 7. To prevent 'damaging' the tubular structure, the users were told to avoid cutting or crushing it with the scalpel.

In the experiments, three control methods were considered. These are listed below, and the details for these three conditions are the same as in Section III-A:

1) **NC** no control, unassisted.
2) **DC3T** 3-D dissipative control in translation.
3) **DC6** full 6-D dissipative control in translation and rotation.

After instruction and training, ten test subjects took part in the experiments, all were right-handed nonsurgeons, aged between 21 and 32. This consisted of eight males and two females. Each subject performed the dissection twice using each of the control methods in a random order. Each trial, after training, lasted 5–6 min on average.

IV. RESULTS

A. Steady-Hand Game

The primary metrics used during the experiment were, the percentage of the pathway for which the ring was in contact, and the root-mean-square error (RMSE) from the optimal ring pose. The interaction power was also recorded as a secondary metric. Results for these metrics are shown in Tables III and IV, and the distributions are plotted in Figs. 8 and 9.

One-way analysis of variance (ANOVA) tests were applied to the results for the primary metrics and they were all found to be significantly affected by the constraint method ($p < 10^{-6}$). Pairwise comparisons were subsequently made between each constraint method pairing using Tukey's honest significant difference (HSD) test for each metric at the 95% confidence interval. The full results from these pairwise comparisons are given in Table V.

B. Soft Tissue Dissection

Four primary metrics were used within the soft tissue dissection experiments to investigate the efficacy of the dissipative controller. These metrics were mean penetration depth of the scalpel into the tube, maximum penetration depth of the scalpel into the tube, mean penetration area of the scalpel within the tube, and displacement of the scalpel while within the tube. As
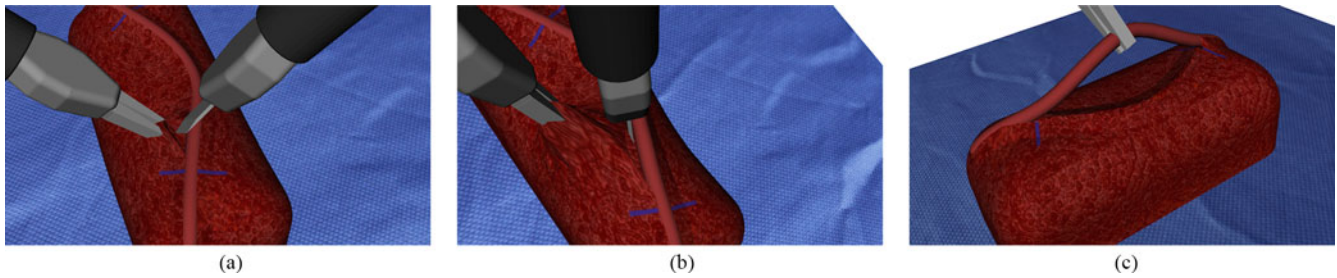
Fig. 7. Dissection process used by the test subjects during the experimental validation. (a) Surface dissection. (b) Subsurface dissection. (c) Completed dissection.

TABLE III
SUMMARY OF THE RESULTS FOR THE SIX CONTROL METHODS IN THE PRIMARY METRICS FOR THE STEADY-HAND GAME EXPERIMENTS

Constraint method	Contact percentage (%)	Translational RMSE (mm)	Rotational RMSE (degrees)
NC	91.1 ± 6.8	10.5 ± 3.8	31.4 ± 8.9
DC3T	34.7 ± 19.6	2.4 ± 0.7	30.1 ± 9.8
DC3R	91.2 ± 6.5	10.8 ± 3.9	29.9 ± 9.6
DC6U	32.5 ± 17.6	2.4 ± 0.7	27.9 ± 8.8
FC6	69.9 ± 19.7	4.7 ± 1.6	30.0 ± 10.1
DC6	7.5 ± 9.0	1.4 ± 0.5	16.2 ± 5.9

Each value shows the mean and standard deviation from a total of 100 tests across 20 test subjects.

TABLE IV
SUMMARY OF THE RESULTS FOR THE SIX CONTROL METHODS IN THE SECONDARY METRICS FOR THE STEADY-HAND GAME EXPERIMENTS

Constraint method	Mean translational power (mW)	Mean rotational power (mW)	Mean total power (mW)
NC	0.0 ± 0.0	0.0 ± 0.0	0.0 ± 0.0
DC3T	−17.5 ± 27.8	0.0 ± 0.0	−17.5 ± 27.8
DC3R	0.0 ± 0.0	−5.0 ± 6.0	−5.0 ± 6.0
DC6U	−16.3 ± 21.5	−16.9 ± 19.9	−33.2 ± 40.0
FC6	−11.2 ± 18.8	−13.4 ± 17.2	−24.6 ± 35.2
DC6	−35.4 ± 46.4	−10.3 ± 15.8	−45.7 ± 54.8

Each value shows the mean and standard deviation from a total of 100 tests across 20 test subjects.

previously, the haptic power was recorded as a secondary metric so that the energetic properties of the constraint methods could be validated. The results for each of the metrics are summarized in Tables VI and VII, and the distributions are plotted in Fig. 10.

As each of the primary metrics was found to be nonnormally distributed by the one-sample Kolmogorov–Smirnov test, the nonparametric Kruskal–Wallis one-way ANOVA test was applied. All four of the primary metrics were found to be significantly affected by the assistance condition ($p < 0.05$). Pairwise comparisons were then made between the means of the three assistance condition pairings using the Dunn–Sidak multiple comparison test, for each primary metric, at the 95% confidence interval. Additionally, pairwise comparisons were made between the variances of the three assistance condition parings using the Brown–Forsythe test, for each primary metric, also at the 95% confidence interval. The results of the Dunn–Sidak and Brown–Forsythe pairwise comparisons are shown in Table VIII.

V. DISCUSSION

A. Steady-Hand Game

The results for the experimental validation of the dissipative controller within the simulated steady-hand game show that it can be of significant benefit to tasks requiring simultaneous accurate movements in multiple dimensions. The only requirement placed upon the user was to keep the ring and pathway from making contact, and therefore, the contact percentage metric quantifies how able they were to do this with the different controllers assisting them.

The results for the no control case (NC) have a high error rate, showing that the task was sufficiently difficulty for robot assis-

tance to be a potential benefit. The contact percentage for the 3-D translational controller (DC3T) was significantly improved, notably with a reduction in translational RMSE, demonstrating that translation only dissipative assistance can be effective, even in tasks requiring rotational control. For the 3-D rotational controller (DC3R) no significant change from NC was found. As dissipative control relies on user energy input, in this case, the user was focusing on translation and did not rotate the device enough to generate assistance.

In the tests where the controller was applied simultaneously, but independently, in translation and rotation (DC6U), the performance was slightly, but not significantly, improved from DC3T. The lack of energy coupling between translation and rotation in DC6U means that, as in DC3R, there is insufficient user energy in rotation to exert significant assistance. When dissipative control was applied without energy redirection (FC6), the performance was improved from the poorest performing cases, NC and DC3R; however, it was worse than the remaining controllers incorporating energy redirection. This result clearly substantiates the hypothesis presented here that energy redirection can improve the fidelity of the assistance offered to such a degree that it improves performance.

The full dissipative controller, which employed energy redirection between all six dimensions (DC6), resulted in the best user performance. When compared with the uncoupled dissipative controller DC6U, this result illustrates the importance of energy redirection between dimensions and those for the power transfer illustrate this further. It can be seen that in some cases, the mean rotational power was actually positive, indicating energetic activity in rotation that was redirected from translation.
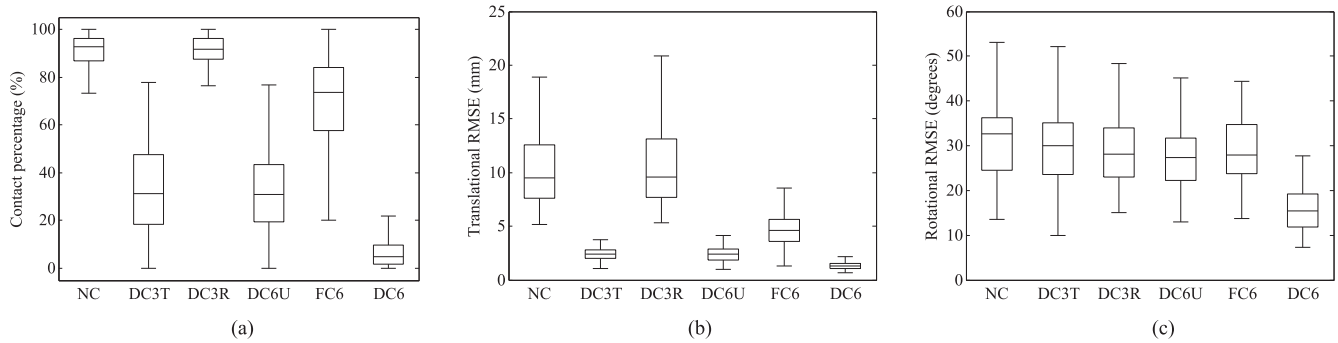
Fig. 8.   Distributions of the results for the six control methods in the primary metrics for the steady-hand game experiments. For clarity, outliers are not shown. (a) Contact percentage. (b) Translational RMSE. (c) Rotational RMSE.
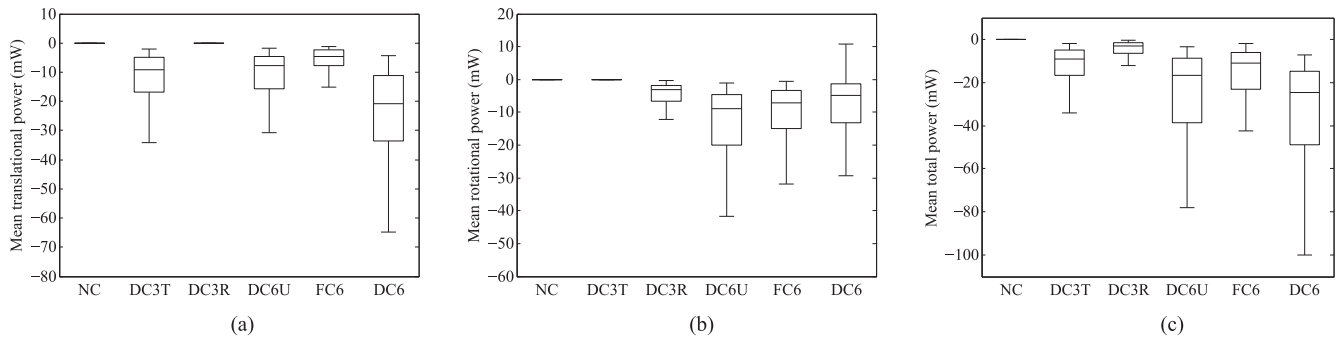

Fig. 9.   Distributions of the results for the six control methods in the secondary metrics for the steady-hand game experiments. For clarity, outliers are not shown. (a) Mean translational power. (b) Mean rotational power. (c) Mean total power.

TABLE V
RESULTS OF TUKEY'S HSD TESTS FOR THE PRIMARY METRICS FOR THE STEADY-HAND GAME EXPERIMENTS

	DC3T	DC3R	DC6U	FC6	DC6
NC	*		*	*	*
DC3T		*		*	*
DC3R			*	*	*
DC6U				*	*
FC6					*

(a) Contact percentage

	DC3T	DC3R	DC6U	FC6	DC6
NC	*		*	*	*
DC3T		*		*	*
DC3R			*	*	*
DC6U				*	*
FC6					*

(b) Translational RMSE

	DC3T	DC3R	DC6U	FC6	DC6
NC					*
DC3T					*
DC3R					*
DC6U					*
FC6					*

(c) Rotational RMSE

TABLE VI
SUMMARY OF THE RESULTS FOR THE THREE CONTROL METHODS IN THE
PRIMARY METRICS FOR THE SOFT TISSUE DISSECTION EXPERIMENTS

Constraint method	Mean penetration depth (μm)	Maximum penetration depth (mm)	Mean penetration area ($\times 10^{-3}$ mm^2)	Contact displacement (mm)
NC	32.8 ± 36.4	0.85 ± 0.24	140.0 ± 168.9	14.3 ± 12.9
DC3T	4.5 ± 7.3	0.46 ± 0.47	19.3 ± 32.6	2.0 ± 3.0
DC6	2.5 ± 5.5	0.38 ± 0.44	13.1 ± 32.1	1.2 ± 2.

Each value shows the mean and standard deviation from a total of 20 tests across 10 test subjects. Note that, due to the circular cross section of the tubular structure, the maximum possible penetration was approximately 1 mm.

TABLE VII
SUMMARY OF THE RESULTS FOR THE THREE CONTROL METHODS IN THE
SECONDARY METRICS FOR THE SOFT TISSUE DISSECTION EXPERIMENTS

Constraint method	Mean translational power (mW)	Mean rotational power (mW)	Mean total power (mW)
NC	0.0 ± 0.0	0.0 ± 0.0	0.0 ± 0.0
DC3T	−1.28 ± 0.57	0.0 ± 0.0	−1.28 ± 0.57
DC6	−1.34 ± 0.57	−2.57 ± 0.95	−3.91 ± 1.40

Each value shows the mean and standard deviation from a total of 20 tests across 10 test subjects.

In all of the test conditions, the total power values shown in Fig. 9 show they are dissipative. The negative power values could potentially have implications for user fatigue. Although intended to be efficient, dissipative control inherently "takes" more energy from the user than an active approach. The degree of fatigue will be formally quantified in future work; nevertheless, as the peak energy dissipation by the controller in all six degrees of freedom is 100 mW (equivalent to 2 N of force at 50 mm/s), and as no users reported physical fatiguing during the experiments, the effect is believed to be small.
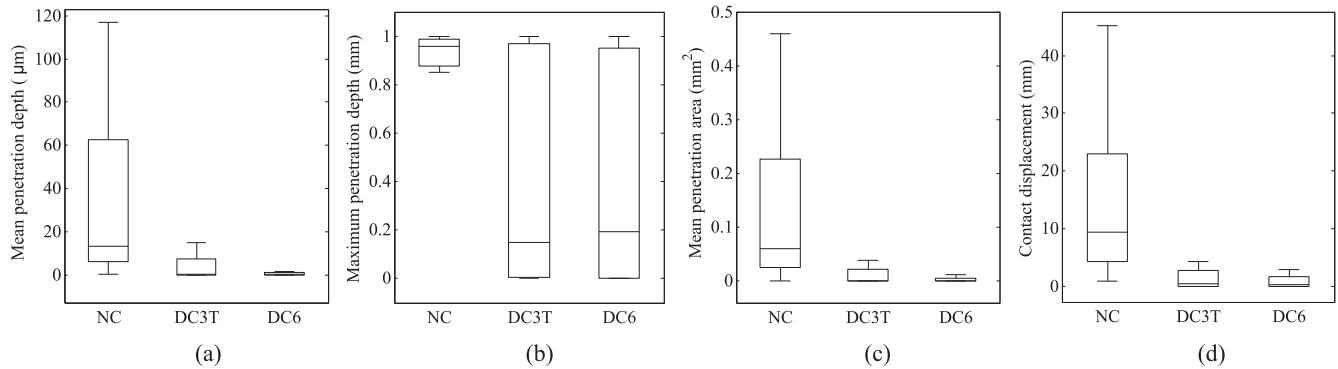
Fig. 10. Distributions of the results for the three control methods in the primary metrics for the soft tissue dissection experiments. For clarity, outliers are not shown. (a) Mean penetration depth. (b) Maximum penetration depth. (c) Mean penetration area. (d) Contact displacement.

TABLE VIII
RESULTS OF PAIRWISE STATISTICAL SIGNIFICANCE TESTS FOR MEANS AND VARIANCES AT THE 95% CONFIDENCE INTERVAL

Constraint method pairing	Mean penetration depth	Maximum penetration depth	Mean penetration area	Contact displacement
NC vs DFC3T	* / •	•	* / •	* / •
NC vs DFC6C	* / •	* / •	* / •	* / •
DFC3T vs DFC6C	•	•	•	•

The symbol "*" identifies a constraint method pairing, and performance metric, with significantly different means. The symbol "•" identifies a constraint method pairing, and performance metric, with significantly different variances.

B. Soft Tissue Dissection

To quantify the effectiveness of the dissipative controller at preventing tissue damage in the dissection task, four metrics were used. The mean and maximum penetration depths identify how deep the user was cutting into the tubular structure during a dissection, the mean penetration area shows how much of the scalpel blade penetrates the tubular structure, and the contact displacement quantifies how far the user moves with the scalpel embedded in the tubular structure. All of these metrics quantify different modes by which the user could cause tissue damage.

Although the motion of the tubular structure was entirely controlled by the users themselves, visualizing the subsurface dissection planes and having the dexterity to follow their intended motion pathway were a challenge for all users, resulting in quantifiable errors with NC. When DC3T was used, the users' performance significantly improved so that most metrics recorded mean and median values near to zero. This shows that even a comparatively simple translational dissipative controller can generally prevent almost all tissue damage in the simulated dissection task. However, there were cases when the users were able to circumvent the DC3T control method, achieving relatively large penetrations or displacements into the tubular structure. These cases typify the primary limitation of a 3-D dissipative controller, which is that a penetration caused by rotation cannot be prevented unless the user is simultaneously translating the tool. The solution to this problem is to implement the full dissipative

controller, DC6. In fact, in the experimental results, DC6 is shown to have the best mean performance across all tissue damage metrics.

The mean performance of DC6 was found to be significantly improved upon NC; however, as the means were so close to zero, it was not found to be significantly improved from DC3T. The Brown–Forsythe tests, however, prove that the variances for DC6 were significantly less than the variances for DC3T. This indicates that, by incorporating the coupled control of orientation, there will be fewer occurrences when the user can accidentally overcome the controller's assistance and damage the tissue, which in a clinical context would represent a significant improvement in itself. Although over 50% of trials had maximum penetrations less than 0.2 mm, the distributions show that some users were still sometimes able to achieve comparatively large maximum penetrations. It is likely that these large penetrations come from occurrences when the tissue was moved toward the motionless scalpel, where a dissipative controller is unable to respond due to the absence of user input. As expected, the total power results for both constraint methods were found to be negative in all cases.

VI. CONCLUSION

This paper has proposed a novel task-space impedance controller that generates unmatched levels of assistance and task performance during physical human–robot interaction, while remaining energetically dissipative. In the case of sensing errors in the robotic system, a conventional active controller can cause sudden, erratic, or even dangerous, movements in the robotic instruments. Conversely, a dissipative controller will ensure that the human user retains overall control of a task, while still receiving the benefits of robotic augmentation, a characteristic which is vitally important in delicate manipulation tasks, such as in robotic surgery.

The control formulation presented is based on the elastoplastic friction model, since friction is a naturally dissipative phenomenon. As friction can only apply forces in directions that oppose the direction of motion, friction-based dissipative controllers conventionally have limited range and fidelity of haptic information. In the controller described here, this problem is

overcome with the use of a new technique called energy redirection. By implementing the elastoplastic friction model within a conical subset of the full n-dimensional space, energy redirection allows the controller to considerably increase performance by taking energy from the user in a dimension in which they are moving and then reintroduce it in another, where control forces are required.

Experimental validation in a 6-D path following task and a simulated surgical dissection demonstrated that the novel advancement of energy redirection was of significant benefit for task accuracy. Both sets of experimental results showed that the full control approach achieved an average 92% reduction in error and clearly verified that the method improves task performance by increasing control fidelity.

The formulation of the controller given in this paper is generalized so that it can be applied to a wide range of robotic applications and tasks. The method has been extensively validated in three and six dimensions; however, in the future, it could readily be applied to higher dimension systems, such as those including haptic controlled forceps.

APPENDIX

A system is dissipative if $\forall t_1 \geq 0$ and $\forall t_2 \geq t_1$:

$$\int_{t_1}^{t_2} s\left(u(t), y(t)\right) dt \geq V(a(t_2)) - V(a(t_1)) \quad (32)$$

where $u(t)$ and $y(t)$ are the system inputs and outputs, respectively, at time t, $s(\cdot)$ is the rate of energy supplied into the system, $V(\cdot)$ is a continuous nonnegative storage function, and $a(t)$ is the system's state variable [4]. The proposed controller conforms to this definition of dissipativity.

Proof: By substituting the interaction power for the supply rate $s(\cdot)$, the elastic presliding potential energy for the storage function $V(\cdot)$, and the elastic presliding displacement for the system state variable $a(t)$ in (32), the above energy inequality subsequently becomes

$$\int_{t_1}^{t_2} \mathbf{f}(t) \cdot \dot{\mathbf{x}}(t) \, dt \geq P\left(\mathbf{z}(t_2)\right) - P\left(\mathbf{z}(t_1)\right). \quad (33)$$

This equality can be proven by demonstrating that $\forall t \geq 0$, the derivative of the supply rate is always greater than the derivative of the storage function:

$$\mathbf{f}(t) \cdot \dot{\mathbf{x}}(t) \geq \frac{d}{dt} P\left(\mathbf{z}(t)\right). \quad (34)$$

Discretizing the inequality at time k and simplifying

$$\mathbf{f}_k \cdot \Delta \mathbf{x}_k \geq P\left(\mathbf{z}_k\right) - P\left(\mathbf{z}_{k-1}\right) \quad (35)$$

where the force applied at a given time step is based on the elastic displacement at the previous time step:

$$\Sigma_0 \mathbf{z}_{k-1} \cdot \Delta \mathbf{x}_k \geq P\left(\mathbf{z}_k\right) - P\left(\mathbf{z}_{k-1}\right). \quad (36)$$

The potential energy of the candidate elastic displacement can be included in the inequality:

$$\Sigma_0 \mathbf{z}_{k-1} \cdot \Delta \mathbf{x}_k \geq P\left(\mathbf{z}_k\right) - P\left(\mathbf{z}_c\right) + P\left(\mathbf{z}_c\right) - P\left(\mathbf{z}_{k-1}\right) \quad (37)$$

or equivalently

$$\Sigma_0 \mathbf{z}_{k-1} \cdot \Delta \mathbf{x}_k \geq \Delta P\left(\mathbf{z}_c, \mathbf{z}_k\right) + \Delta P\left(\mathbf{z}_{k-1}, \mathbf{z}_c\right) \quad (38)$$

where $\Delta P\left(\cdot, \cdot\right) : \mathbb{R}^n \times \mathbb{R}^n \to \mathbb{R}$ is the change in potential energy between two elastic presliding displacements, i.e.,

$$\Delta P\left(\mathbf{a}, \mathbf{b}\right) = P\left(\mathbf{b}\right) - P\left(\mathbf{a}\right) \quad (39)$$

where $\mathbf{a}, \mathbf{b} \in \mathbb{R}^n$ are arbitrary multidimensional elastic displacement vectors.

Under the assumption that $\mathbf{z}_{k-1}$ and $\Delta \mathbf{x}_k$ are sufficiently small that the candidate elastic presliding displacement can be approximated linearly:

$$\mathbf{z}_c = \mathbf{z}_{k-1} + \Delta \mathbf{x}_k \quad (40)$$

(39), therefore, becomes

$$\Delta P\left(\mathbf{z}_{k-1}, \mathbf{z}_c\right) = P\left(\mathbf{z}_{k-1} + \Delta \mathbf{x}_k\right) - P\left(\mathbf{z}_{k-1}\right). \quad (41)$$

Substituting in the definition for $P\left(\cdot\right)$ and canceling gives

$$\Delta P\left(\mathbf{z}_{k-1}, \mathbf{z}_c\right) = \Sigma_0 \mathbf{z}_{k-1} \cdot \Delta \mathbf{x}_k + \frac{1}{2} \Sigma_0 \Delta \mathbf{x}_k \cdot \Delta \mathbf{x}_k. \quad (42)$$

Substituting (42) into the dissipativity criterion in (38) and canceling

$$0 \geq \Delta P\left(\mathbf{z}_c, \mathbf{z}_k\right) + \frac{1}{2} \Sigma_0 \Delta \mathbf{x}_k \cdot \Delta \mathbf{x}_k \quad (43)$$

where $\frac{1}{2} \Sigma_0 \Delta \mathbf{x}_k \cdot \Delta \mathbf{x}_k$ is the standard discretization error inherent in discrete simulations of elastic springs. This component is considered to be negligible given the assumption that the control frequency is sufficiently high in relation to the movement speed.

The dissipativity inequality subsequently becomes

$$P\left(\mathbf{z}_c\right) \geq P\left(\mathbf{z}_k\right). \quad (44)$$

As the computation of $\mathbf{z}_k$ from $\mathbf{z}_c$ in (26) is expressed in the potential energy space, it is necessary to define a function $\tilde{P}$, which computes the potential energy stored in the system based on the potential energy mapped elastic presliding displacement, such that

$$\tilde{P}(\tilde{\mathbf{z}}_c) \geq \tilde{P}(\tilde{\mathbf{z}}_k). \quad (45)$$

The function $\tilde{P}$ is defined as follows and can be proven by expanding the elementwise dot products as

$$P\left(\mathbf{a}\right) = \tilde{P}(M(\mathbf{a})) = \tilde{P}(\tilde{\mathbf{a}}) = \|\tilde{\mathbf{a}}\|^2 = \tilde{\mathbf{a}} \cdot \tilde{\mathbf{a}}. \quad (46)$$

Proof that the proposed controller is dissipative, as defined in (45), is given in two parts. Initially, this is proven when $\tilde{\mathbf{z}}_k$ is computed from $\tilde{\mathbf{z}}_c$ using the first and second subfunctions of (26), i.e., when

$$\tilde{\mathbf{z}}_k = \beta \tilde{\mathbf{z}}_c, \quad \text{where} \quad 0 \leq \beta \leq 1. \quad (47)$$

Substituting this definition into (45) with the definition for $\tilde{P}$ gives

$$\tilde{P}(\tilde{\mathbf{z}}_c) \geq \tilde{P}(\beta \tilde{\mathbf{z}}_c) \quad (48)$$

$$1 \geq \beta \quad (49)$$

which conforms to the definition of β in (47).

Finally, the dissipativity inequality is proven for the third subfunction of (26), i.e., when

$$\tilde{\mathbf{z}}_k = \gamma((\tilde{\mathbf{z}}_c \cdot \hat{\mathbf{y}})\hat{\mathbf{y}}), \quad \text{where} \quad 0 \le \gamma \le 1. \tag{50}$$

Substituting this definition into (45) gives

$$\tilde{P}(\tilde{\mathbf{z}}_c) \ge \tilde{P}(\gamma((\tilde{\mathbf{z}}_c \cdot \hat{\mathbf{y}})\hat{\mathbf{y}})) \tag{51}$$

$$1 \ge \gamma \tag{52}$$

which conforms to the definition of γ in (50). ■

REFERENCES

[1] R. Taylor, P. Jensen, L. Whitcomb, A. Barnes, R. Kumar, D. Stoianovici, P. Gupta, Z. Wang, E. Dejuan, and L. Kavoussi, "A steady-hand robotic system for microsurgical augmentation," *Int. J. Robot. Res.*, vol. 18, no. 12, pp. 1201–1210, 1999.

[2] M. A. Peshkin, J. E. Colgate, W. Wannasuphoprasit, C. A. Moore, R. B. Gillespie, and P. Akella, "Cobot architecture," *IEEE Trans. Robot. Autom.*, vol. 17, no. 4, pp. 377–390, Aug. 2001.

[3] A. De Santis, B. Siciliano, A. D. Luca, and A. Bicchi, "An atlas of physical humanrobot interaction," *Mechanism Mach. Theory*, vol. 43, pp. 253–270, 2008.

[4] J. C. Willems, "Dissipative dynamical systems," *Euro. J. Control*, vol. 13, pp. 134–151, 2007.

[5] J. C. Willems, "Dissipative dynamical systems—Part I: General theory," *Archive Rational Mech. Anal.*, vol. 45, no. 5, pp. 321–351, 1972.

[6] S. A. Bowyer, B. L. Davies, and F. R. Y. Baena, "Active constraints/virtual fixtures: A survey," *IEEE Trans. Robot.*, vol. 30, no. 1, pp. 138–157, Feb. 2014.

[7] L. B. Rosenberg, "Virtual fixtures: Perceptual tools for telerobotic manipulation," in *Proc. IEEE Virtual Reality Annu. Int. Symp.*, Sep. 1993, pp. 76–82.

[8] M. Li, M. Ishii, and R. H. Taylor, "Spatial motion constraints using fixtures generated by anatomy," *IEEE Trans. Robot.*, vol. 23, no. 1, pp. 4–19, Feb. 2007.

[9] M. Jakopec, F. R. Y. Baena, S. Harris, P. Gomes, J. Cobb, and B. L. Davies, "The hands-on orthopaedic robot "Acrobot": Early clinical trials of total knee replacement surgery," *IEEE Trans. Robot. Autom.*, vol. 19, no. 5, pp. 902–911, Oct. 2003.

[10] F. R. Y. Baena and B. Davies, "Robotic surgery: From autonomous systems to intelligent tools," *Robotica*, vol. 28, no. 2, pp. 163–170, Mar. 2010.

[11] A. Bicchi, M. A. Peshkin, and J. E. Colgate, "Safety for physical human-robot interaction," in *Springer Handbook of Robotics*, B. Siciliano and O. Khatib, Eds., Berlin, Germany: Springer 2008, pp. 1335–1348.

[12] G. Hirzinger, A. Albu-Schaffer, M. Hahnle, I. Schaefer, and N. Sporer, "On a new generation of torque controlled light-weight robots," in *Proc. IEEE Int. Conf. Robot. Autom.*, 2001, vol. 4, pp. 3356–3363.

[13] M. Zinn, O. Khatib, B. Roth, and J. Salisbury, "Playing it safe," *IEEE Robot. Autom. Mag.*, vol. 11, no. 2, pp. 12–21, Jun. 2004.

[14] R. Alami, A. Albu-Schaeffer, A. Bicchi, R. Bischoff, R. Chatila, A. De Luca, A. De Santis, G. Giralt, J. Guiochet, G. Hirzinger, F. Ingrand, V. Lippiello, R. Mattone, D. Powell, S. Sen, B. Siciliano, G. Tonietti, and L. Villani, "Safe and dependable physical human-robot interaction in anthropic domains: State of the art and challenges," in *Proc. IEEE/RSJ Int. Conf. Intell. Robot. Syst.*, Oct. 2006, pp. 1–16.

[15] J. Troccaz and Y. Delnondedieu, "Semi-active guiding systems in surgery. A two-dof prototype of the passive arm with dynamic constraints (PADyC)," *Mechatronics*, vol. 6, no. 4, pp. 399–421, 1996.

[16] W. Book, R. Charles, H. Davis, and M. Gomes, "The concept and implementation of a passive trajectory enhancing robot," in *Proc. Int. Mech. Eng. Congr. Expo.*, Atlanta, GA, USA, Nov. 1996, pp. 633–638.

[17] R. Kikuuwe, N. Takesue, and H. Fujimoto, "A control framework to generate nonenergy-storing virtual fixtures: Use of simulated plasticity," *IEEE Trans. Robot.*, vol. 24, no. 4, pp. 781–793, Aug. 2008.

[18] R. Prada and S. Payandeh, "On study of design and implementation of virtual fixtures," *Virtual Reality*, vol. 13, no. 2, pp. 117–129, Jun. 2009.

[19] P. Aigner and B. McCarragher, "Human integration into robot control utilising potential fields," in *Proc. IEEE Int. Conf. Robot. Autom.*, Apr. 1997, vol. 1, pp. 291–296.

[20] D. Hennekens, D. Constantinescu, and M. Steinbuch, "Continuous impulsive force controller for forbidden-region virtual fixtures," in *Proc. IEEE Int. Conf. Robot. Autom.*, May 2008, pp. 2890–2895.

[21] P. Marayong, M. Li, A. M. Okamura, and G. D. Hager, "Spatial motion constraints: Theory and demonstrations for robot guidance using virtual fixtures," in *Proc. IEEE Int. Conf. Robot. Autom.*, 2003, pp. 1954–1959.

[22] S. A. Bowyer and F. R. Y. Baena, "Dynamic frictional constraints for robot assisted surgery," in *Proc. IEEE World Haptics Conf.*, 2013, pp. 319–324.

[23] S. A. Bowyer and F. R. Y. Baena, "Dynamic frictional constraints in translation and rotation," in *Proc. IEEE Int. Conf. Robot. Autom.*, 2014, pp. 2685–2692.

[24] P. Dupont, V. Hayward, B. Armstrong, and F. Altpeter, "Single state elastoplastic friction models," *IEEE Trans. Autom. Control*, vol. 47, no. 5, pp. 787–792, May 2002.

[25] P. Dahl, "A solid friction model," Aerospace Corp., El Segundo, CA, USA, Tech. Rep. TOR-0158(3107-18)-1, 1968.

[26] C. Canudas de Wit, H. Olsson, K. Astrom, and P. Lischinsky, "A new model for control of systems with friction," *IEEE Trans. Autom. Control*, vol. 40, no. 3, pp. 419–425, Mar. 1995.

[27] V. Hayward, B. S. R. Armstrong, F. Altpeter, and P. E. Dupont, "Discrete-time elasto-plastic friction estimation," *IEEE Trans. Control Syst. Technol.*, vol. 17, no. 3, pp. 688–696, May 2009.

[28] T. Yoshikawa, "Dynamic manipulability of robot manipulators," in *Proc. IEEE Int. Conf. Robot. Autom.*, Mar. 1985, vol. 2, pp. 1033–1038.

[29] B. Brogliato, R. Lozano, B. Maschke, and O. Egeland, *Dissipative Systems Analysis and Control. Theory and Applications* (ser. Communications and Control Engineering), 2nd ed. New York,NY, USA: Springer, 2007.

[30] R. J. Adams and B. Hannaford, "Stable haptic interaction with virtual environments," *IEEE Trans. Robot. Autom.*, vol. 15, no. 3, pp. 465–474, Jun. 1999.

[31] D. Hill and P. Moylan, "The stability of nonlinear dissipative systems," *IEEE Trans. Autom. Control*, vol. AC-21, no. 5, pp. 708–711, Oct. 1976.

[32] N. Hogan, "Controlling impedance at the man/machine interface," in *Proc. IEEE Int. Conf. Robot. Autom.*, May 1989, vol. 3, pp. 1626–1631.

[33] H. Bruyninckx, "Open robot control software: The OROCOS project," in *Proc. IEEE Int. Conf. Robot. Autom.*, 2001, vol. 3, pp. 2523–2528.

[34] M. Ortega, S. Redon, and S. Coquillart, "A six degree-of-freedom god-object method for haptic display of rigid bodies with surface properties," *IEEE Trans. Vis. Comput. Graphics*, vol. 13, no. 3, pp. 458–469, May 2007.

[35] S. A. Bowyer and F. R. Y. Baena, "Deformation invariant bounding spheres for dynamic active constraints in surgery," *Proc. Inst. Mech. Eng., Part H, J. Eng. Med.*, vol. 228, no. 4, pp. 350–361, Apr. 2014.

[36] J. Allard, S. Cotin, F. Faure, P.-J. Bensoussan, F. Poyer, C. Duriez, H. Delingette, and L. Grisoni, "SOFA—An open source framework for medical simulation," in *Medicine Meets Virtual Reality*. Long Beach, CA, USA: IOP Press, Feb. 2007.

Stuart A. Bowyer (S'11–M'14) received the B.Eng. degree in mechanical engineering from Loughborough University, Loughborough, U.K. in 2007, the M.Sc. degree in computer science from the University of Oxford, Oxford, U.K. in 2010, and the Ph.D. degree in medical robotics from Imperial College London, London, U.K. in 2014.

Ferdinando Rodriguez y Baena (M' 09) received the M.Eng. degree in mechatronics and manufacturing systems engineering from King's College London, London, U.K., in 2000 and the Ph.D. degree in medical robotics from Imperial College London, London, in 2004.

He is a Reader in medical robotics with the Department of Mechanical Engineering, Imperial College London, where he leads the Mechatronics in Medicine Laboratory. His research interests include mechatronic systems for diagnostics, surgical training, and intervention.